Spacecraft Wall Design for Increased Protection Against Penetration by Orbital Debris Impacts

William P. Schonberg*
University of Alabama in Huntsville, Huntsville, Alabama 35899
and
Randy J. Tullos†
Southwest Research Institute, San Antonio, Texas 78284

All orbiting spacecraft are susceptible to impacts by meteoroids and pieces of orbital space debris. These impacts occur at extremely high speeds and can damage flight-critical systems, which can in turn lead to catastrophic failure of the spacecraft. The design of a spacecraft for a long-duration mission into the meteoroid and space debris environment must include adequate protection against perforation of pressurized components by such impacts. This paper presents the results of an investigation into the perforation resistance of dual-wall structural systems fabricated with monolithic bumper plates and with corrugated bumper plates of equal weight. A comparative analysis of the impact damage in dual-wall systems with corrugated bumper specimens and that in dual-wall specimens with monolithic bumpers of similar weight is performed to determine the advantages and disadvantages of employing corrugated bumpers in structural wall systems for long-duration spacecraft. The analysis indicates that a significant increase in perforation protection can be achieved if a monolithic bumper is replaced by a corrugated bumper of equal weight. The parameters of the corrugations in the corrugated bumper plates are optimized in a manner that minimizes the potential for the creation of ricochet debris in the event of an oblique hypervelocity impact. Several design examples using the optimization scheme are presented and discussed.

Introduction

THE walls of a spacecraft developed for a mission into the meteoroid and orbital debris environment must be designed to resist perforation by meteoroids and pieces of orbital debris. On-orbit impacts by these high-speed particles can damage the flight-critical systems of a spacecraft, which can in turn lead to catastrophic failure. Traditional perforation-resistant wall design for long-duration spacecraft consists of a bumper plate that is placed at a small distance away from the main pressure wall of the compartment or module. This concept was first proposed by Whipple[1] and has been studied extensively in the last three decades as a means of reducing the perforation threat of hypervelocity projectiles (see, e.g., Refs. 2–16). In the majority of these investigations, the bumper plates were typically uniform in nature and made from a variety of metallic or composite materials. Dual-wall configurations were repeatedly shown to provide significant increases in protection against perforation by small high-speed projectiles over equivalent single-wall structures. However, the recent proliferation of large pieces of orbital debris has made it necessary to modify such systems so that they can resist penetration by projectiles with much higher impact energies. Novel design concepts that possess increased levels of protection must be developed for spacecraft that are to be launched into the meteoroid and orbital debris environment.

In the first part of this paper, the results of hypervelocity impact experiments are presented and discussed. In these experiments, a modified dual-wall structural system was tested for perforation by hypervelocity projectiles. In this modified system, the traditional uniform bumper was replaced by a corrugated bumper of equal weight. Impact test results for two different types of corrugated bumpers are reviewed qualitatively and quantitatively. Impact damage in the structural systems is characterized according to the extent of perforation, crater, and spall damage in the pressure wall plate as a result of the impact loadings. The impact damage in the specimens with corrugated bumper plates is compared to impact damage in specimens with uniform, monolithic bumpers of similar weight. This comparative analysis is used to determine the advantages and disadvantages of employing corrugated bumpers in structural wall systems for long-duration spacecraft.

In the second part of the paper, a novel variation of the standard corrugated bumper plate configuration is presented. It is shown that the corrugation parameters in the proposed modified configuration can be optimized in a manner that minimizes the creation of ricochet debris in the event of an oblique debris particle impact. The optimization scheme developed is applicable to a wide variety of space structures, including the Space Station Freedom. Several design examples using the optimization scheme are presented and discussed.

Hypervelocity Impact Testing of Dual-Wall Systems

The high-speed impact testing of the structural systems was performed at the Space Debris Impact Facility of the Materials and Processes Laboratory at the NASA Marshall Space Flight Center.[17] In each test, a projectile of diameter d and velocity V impacted a dual-wall test specimen along a trajectory inclined at an angle θ with respect to the outward normal of the test specimen bumper plate. Figure 1 illustrates the oblique impact of a dual-wall test specimen with a monolithic bumper plate (a "monolithic bumper system"), whereas Fig. 2 shows the oblique impact of a dual-wall system with a corrugated bumper (a "corrugated bumper system"). In Fig. 2, the corrugated bumper is seen to consist of a series of corrugations sandwiched in between flat "front" and "rear" bumper plates, where the front plate is that plate that is first struck by an incoming projectile.

In the monolithic bumper system impacts, the projectile was shattered and created a hole in the bumper plate. In the corrugated system impacts, a series of holes were created in the corrugations as the debris cloud containing projectile and

Received Nov. 9, 1990; revision received May 21, 1991; accepted for publication May 29, 1991. Copyright © 1991 by the American Institute of Aeronautics and Astronautics, Inc. All rights reserved.

*Associate Professor, Civil Engineering Program.
†Senior Research Engineer.

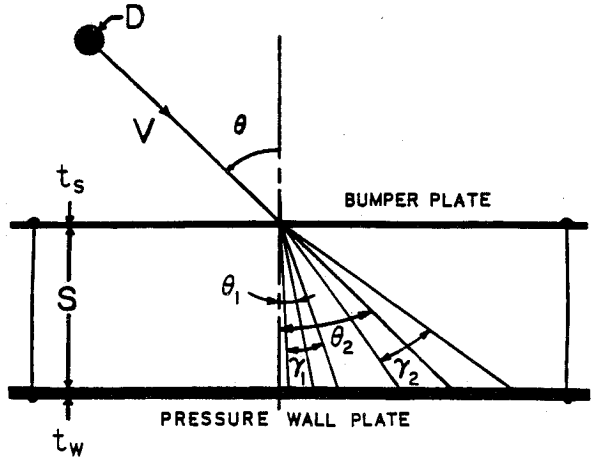

Fig. 1 Impact test configuration and parameters for the monolithic bumper system.

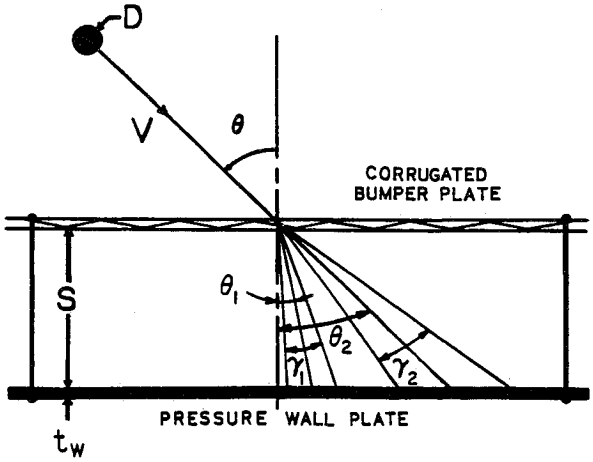

Fig. 2 Impact test configuration and parameters for the corrugated bumper system.

bumper plate fragments spread out and moved through the corrugations. In both cases, the secondary debris fragments were sprayed upon a pressure wall plate of thickness t_w located a distance S behind the bumper plate. In the corrugated bumper systems, the distance S is measured from the pressure wall plate to the rear plate of the corrugated bumper. In Figs. 1 and 2, the angles θ_1 and θ_2 denote the trajectories of the centers of mass of the "normal" and "in-line" secondary debris fragments, respectively; the angles γ_1 and γ_2 represent the spread of these fragments. It is noted that the spread of the secondary debris clouds in the corrugated bumper systems began immediately so that by the time the debris cloud exited the rear of the bumper, a fair amount of spreading had already occurred. Therefore, the angles θ_1, θ_2 and γ_1, γ_2 for the corrugated bumper systems are measured from the impact site on the front plate and not from the debris cloud exit site on the rear plate. The impact of the secondary debris particles created normal and in-line areas of damage A_{d1} and A_{d2}, respectively, on the front surface of the pressure wall plate. In those tests where the path of the projectile was normal to the surface of the bumper plate (i.e., $\theta = 0$ deg), the normal and in-line debris clouds overlapped in a single debris cloud whose center-of-mass trajectory was close to the inward normal of the test specimen bumper plate (i.e., $\gamma_1 \simeq \gamma_2 = \gamma_n$ and $\theta_1 \simeq \theta_2 = \theta_n$). The damage areas also overlapped and combined to form a single area of damage A_d on the front surface of the pressure wall plate. Occasionally, the impacts

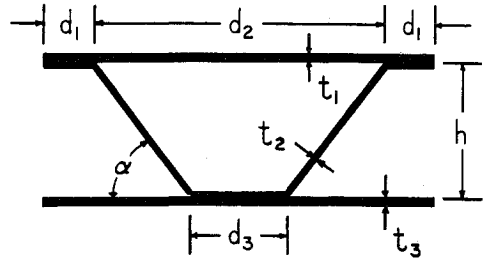

Fig. 3 Corrugated bumper repeating element.

of the secondary projectile and bumper plate fragments resulted in the creation of thin spall fragments ejected from the rear side of the pressure wall plate. In these cases, for both the normal and oblique impacts, the total spalled area on the rear surface is denoted by A_s.

The conditions of the impact tests were chosen to simulate orbital debris impacts of light-weight space structures as closely as possible, and still remain within the realm of experimental feasibility. Kessler et al., state that the average mass density for pieces of orbital debris less than 10 mm in diameter is approximately the same as that of aluminum.[18] Although it is anticipated that the shape of the impacting projectile will affect impact damage formation and propagation,[19] spherical projectiles were used in the test program to maintain repeatability and consistency. Thus, the testing was conducted with solid spherical 1100 aluminum projectiles with diameters ranging from 6.35 to 9.53 mm. The velocities of the impacting projectiles ranged from 2.9 to 7.0 km/s. To study the effects of trajectory obliquity on perforation, impact testing was performed at obliquities of 0 deg and 45 deg. Additionally, to simulate presence of thermal insulation in the spacecraft wall design, some of the tests were performed with multi-layer insulation (MLI) resting on the pressure wall plate.

A total of 15 structural systems with monolithic bumper plates and 13 systems with corrugated bumper plates were used to evaluate the perforation resistance of dual-wall systems with corrugated bumpers. In both systems, the bumper and pressure wall plates were made from 6061-T6 and 2219-T87 aluminum, respectively. Two different types of corrugated bumper plates were used: one consisted of "deep" corrugations with a repeating element rise angle $\alpha = 53$ deg; the other consisted of "shallow" corrugations with a repeating element rise angle of $\alpha = 20$ deg (see Fig. 3). Additional dimensions of the repeating element of the corrugated bumpers considered in this study are given in Table 1. The thicknesses of the monolithic bumper plates were chosen such that the monolithic and corrugated bumper plates had similar areal densities. The corrugated bumper plates were calculated to have areal densities of approximately 0.456 g/cm^2; therefore, dual-wall systems with monolithic bumper plates 1.6 mm thick were used for comparison. The MLI consisted of 30 layers of 0.5-mil kapton aluminized on one side and 29 layers of Dacron mesh between each kapton layer. One layer of beta-cloth (coated s-glass) was added on the side nearest the bumper plate for durability. The areal density of this combination was calculated to be approximately 0.107 g/cm^2.[8] Additional test parameters and configuration geometries are given in Table 2 for the high-speed impact tests. In Table 2, the final group of monolithic bumper system tests were performed to allow a more accurate monolithic bumper system perforation curve to be drawn.

The results of the impact tests are given in Tables 3 and 4. In these tables, the results are presented for tests grouped according to both geometric and impact energy similarity. The results of the additional monolithic bumper system tests are given at the bottom of Table 4. Column entries of "—" indicate that certain phenomena, such as pressure wall plate perforation, did not occur. Additionally, d_h is the equivalent

hole diameter of all the holes in the pressure wall plate in the event of pressure wall plate perforation. Perforation curves for the structural systems under oblique impact are presented in Fig. 4. It is noted that these curves are merely lines of demarcation between regions of perforation (above) and no perforation (below). Detailed inspection and analysis of the damaged test specimens revealed many interesting features and response characteristics of dual-wall structures with corrugated bumper plates. Figures 5 through 9 show typical damaged corrugated and monolithic bumper systems.

Hypervelocity Impact Response Characteristics

Bumper Damage Analysis

The impact damage in the monolithic bumper plates and the flat front plates of the corrugated bumpers consisted of either a circular or an elliptical hole, depending on the trajectory obliquity. As the impact obliquity was increased from 0 deg to 45 deg, the hole became noticeably elongated. In the tests with the corrugated bumper plates, a significant number of the debris fragments were trapped within the corrugations and did not exit the rear bumper panel. Therefore, the amount of energy imparted to the pressure wall plate by the debris clouds in the tests with the corrugated bumpers was much lower than that imparted to the pressure wall by the debris clouds in the tests with monolithic bumper plates. Side and rear views of a normally impacted corrugated bumper plate are shown in Figs. 5a and 5b, respectively. Although Fig. 5b shows a large exit hole, Figs. 5a and 5b show that a fair amount of petalling of the flat "rear" plate has occurred. This implies that a large portion of the energy of the bumper fragments went into deforming the rear plate rather than creating additional secondary debris.

Table 1 Geometric parameters for corrugated bumpers

	Corrugation type No. 1	Corrugation type No. 2
α	53 deg	20 deg
h	19.0	25.4
t_1	0.508	0.803
t_2	0.508	0.508
t_3	0.508	0.508
d_1	7.938	3.175
d_2	44.450	146.050
d_3	15.875	6.350

Note: All lengths and thicknesses in mm.

Pressure Wall Plate Damage Analysis

In Tables 3 and 4, impact test results are presented for tests grouped according to geometric and impact energy similarity. Perforation curves for the structural systems with shallow corrugated bumpers and the corresponding systems with traditional monolithic bumper plates are shown in Fig. 4. Using Tables 3 and 4 and the perforation curves in Fig. 4, an in-depth comparison of hypervelocity impact response characteristics was performed.

In Table 3 (i.e., under normal impact), the pressure wall plate damage areas and debris cloud cone angles of the systems with monolithic bumper plates were much larger than those in the corresponding dual-wall systems with corrugated bumper plates. Additionally, in Table 3, pressure wall plate perforation is seen to occur in all three corrugated bumper systems and in almost all of the systems with monolithic bumper plates. Although the likelihood of perforation under normal impact appears to be the same for both types of systems, it is important to note that the reverse sides of the pressure wall plates of the corrugated bumper systems did not exhibit any spall, while those of the monolithic bumper systems exhibited significant rear-side spalling (see Fig. 7b). This increased tendency for spall in the monolithic bumper specimens is a direct consequence of the wider areal distribution of the impulse delivered by the secondary debris fragment cloud. The impulse delivered to the pressure wall plate in the corrugated

Table 2 Hypervelocity impact test parameters

Test number	α, deg	V, km/s	θ, deg	d, mm	MLI?	t_w, mm	S, cm
			Corrugated bumper systems				
145A	53	5.40	0	6.35	N	3.175	10.16
145B	53	4.38	0	6.35	N	3.175	10.16
145C	53	3.79	0	6.35	N	3.175	10.16
307	20	2.96	45	6.35	Y	3.175	10.16
308	20	4.42	45	6.35	Y	3.175	10.16
309	20	4.60	45	7.95	Y	3.175	10.16
309B	20	4.86	45	7.95	Y	3.175	10.16
309R	20	4.56	45	7.95	Y	3.175	10.16
310	20	5.73	45	7.95	Y	3.175	10.16
310R	20	5.78	45	7.95	Y	3.175	10.16
311	20	5.29	45	9.53	Y	3.175	10.16
312	20	6.08	45	9.53	Y	3.175	10.16
312B	20	6.52	45	9.53	Y	3.175	10.16
			Monolithic bumper systems				
EHSS2B	—	5.88	0	6.35	N	3.175	10.16
P03	—	4.90	0	6.35	N	3.175	10.16
P04	—	4.95	0	6.35	N	3.175	10.16
PT4A	—	3.64	0	6.35	N	3.175	10.16
PT4B	—	4.26	0	6.35	N	3.175	10.16
205A	—	4.16	45	6.35	Y	3.175	10.16
205B	—	4.61	45	6.35	Y	3.175	10.16
205D	—	6.30	45	6.35	Y	3.175	10.16
205E	—	3.15	45	6.35	Y	3.175	10.16
211D	—	6.97	45	8.89	Y	3.175	10.16
212B	—	6.27	45	7.62	Y	3.175	10.16
230A	—	4.41	45	4.75	Y	3.175	10.16
325	—	4.25	45	7.95	Y	3.175	10.16
205C	—	5.30	45	6.35	Y	3.175	10.16
230B	—	3.23	45	4.75	Y	3.175	10.16

Table 3 Comparison of corrugated and monolithic bumper systems under normal hypervelocity impact

Test number	System type	Impact energy, J	θ_n, deg	γ_n, deg	A_d, cm^2	d_h, mm	A_s, cm^2
145A	CBS[a]	5,302	1.5	26.6	25.67	2.87	—
EHSS2B	MBS[b]	6,287	0.0	47.3	62.06	—	5.19
145B	CBS	3,489	0.2	24.8	22.06	2.28	—
PT4B	MBS	3,300	6.9	49.1	64.58	16.01	3.94
P03	MBS	4,366	1.4	48.4	81.03	9.09	3.44
P04	MBS	4,456	0.7	48.1	64.58	7.72	1.97
145C	CBS	2,612	1.6	33.5	41.87	7.29	—
PT4A	MBS	2,409	1.4	57.5	69.48	6.35	0.26

[a]CBS, corrugated bumper system; [b]MBS, monolithic bumper system.

Table 4 Comparison of corrugated and monolithic bumper systems under oblique hypervelocity impact

Test number	System type[a]	Impact energy, J	θ_1, deg	θ_2, deg	γ_1, deg	γ_2, deg	A_{d1}, cm^2	A_{d2}, cm^2	d_h, mm
307	CBS	1,593	—	40.7	—	3.3	—	1.29	—
205E	MBS	1,804	8.5	37.3	14.0	4.5	5.10	1.29	8.79
230A	MBS	1,480	5.7	42.5	20.9	3.0	11.42	0.71	—
308	CBS	3,552	28.4	38.7	13.2	7.4	9.55	6.39	—
205A	MBS	3,147	9.9	41.2	32.3	10.8	28.58	7.94	2.44
205B	MBS	3,864	12.7	40.4	23.3	14.1	15.55	17.81	4.37
309	CBS	7,551	20.3	37.6	13.7	13.0	7.94	17.81	2.98
309B	CBS	8,429	13.5	33.8	5.5	12.8	1.29	13.36	—
309R	CBS	7,420	16.7	38.7	15.3	5.3	11.42	2.84	—
205D	MBS	7,217	8.5	35.7	17.4	9.2	7.92	5.10	—
325	MBS	6,446	11.3	41.2	27.7	10.9	20.26	7.94	14.17
310	CBS	11,716	—	35.6	—	6.7	—	3.87	—
310R	CBS	11,922	32.6	49.8	20.5	2.4	25.68	1.29	—
212B	MBS	12,353	5.4	38.0	14.1	15.9	5.10	17.80	15.75
311	CBS	24,221	12.0	39.7	22.1	8.7	20.25	7.94	18.67
312	CBS	22,687	—	42.0	—	10.7	—	14.52	—
312B	CBS	26,089	—	21.8	—	22.8	—	25.68	15.37
211D	MBS	24,240	—	40.2	—	11.8	—	11.42	38.18
205C	MBS	5,107	19.3	37.9	15.9	12.1	7.92	9.58	16.94
230B	MBS	794	7.1	40.1	7.1	6.8	1.29	3.87	—

[a]CBS, corrugated bumper system; MBS, monolithic bumper system.

bumper systems appears to be more concentrated (compare Fig. 6 with Fig. 7a). However, the smaller damage areas are actually due to the fewer number of debris particles in the secondary debris clouds. This resulted in a decreased tendency for rear-side spall in the corrugated bumper systems.

Under oblique impact in the presence of MLI, neither system exhibited rear-side pressure wall plate spallation. This is probably a function of the presence of the MLI rather than the obliquity of impact. In a previous investigation of hypervelocity impact, it was found that rear-side pressure wall plate spall could occur in dual-wall systems under oblique as well as normal impact conditions.[8] Perforation of the pressure wall plate was found to occur in all but three (i.e., in 70%) of the systems with monolithic bumpers. However, only three (i.e., 30%) of the corrugated bumper systems sustained pressure wall plate perforation. Furthermore, the equivalent hole diameters of the pressure wall plates in the perforated corrugated bumper systems were typically smaller than those in the corresponding monolithic bumper systems (see Table 4 and compare Fig. 8 with Fig. 9). Thus, while pressure wall plate

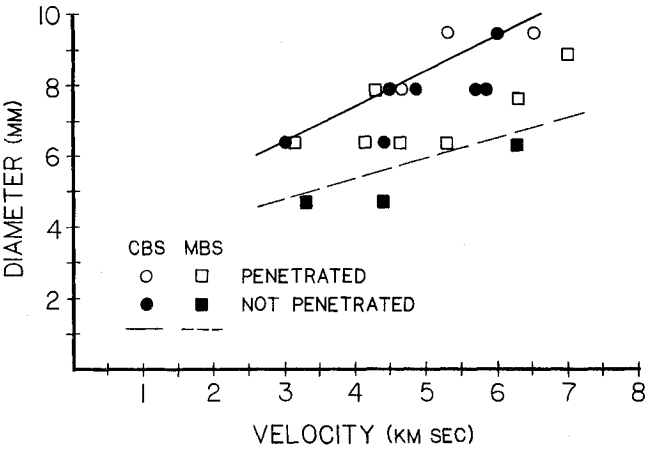

Fig. 4 Penetration functions for corrugated and monolithic bumper systems with MLI (corrugated bumper system—CBS, monolithic bumper system—MBS) for θ = 45 deg and α = 20 deg.

a)

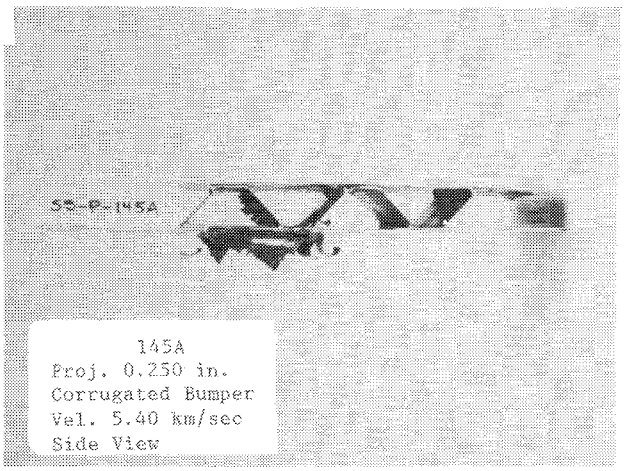

b)

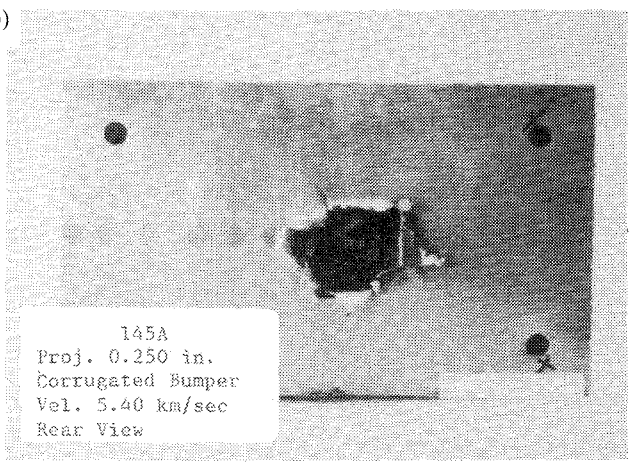

Fig. 5 Corrugated bumper plate under normal impact: a) side view; b) rear view.

a)

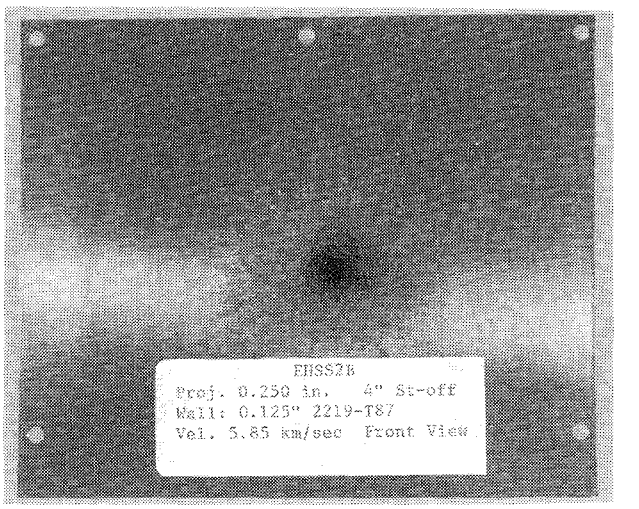

b)

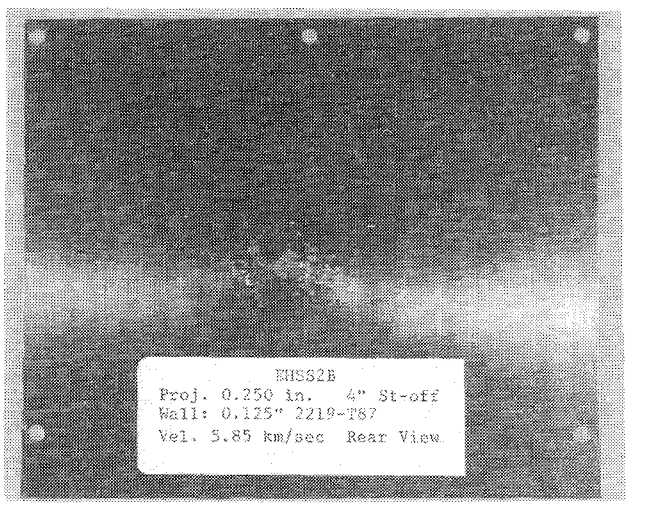

Fig. 7 Pressure wall plate of a monolithic bumper system under normal impact: a) front view; b) rear view.

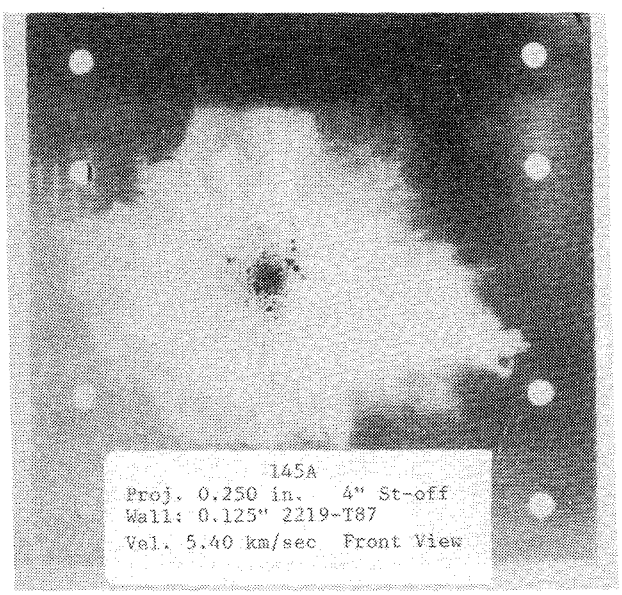

Fig. 6 Front view of a pressure wall plate of a corrugated bumper system under normal impact.

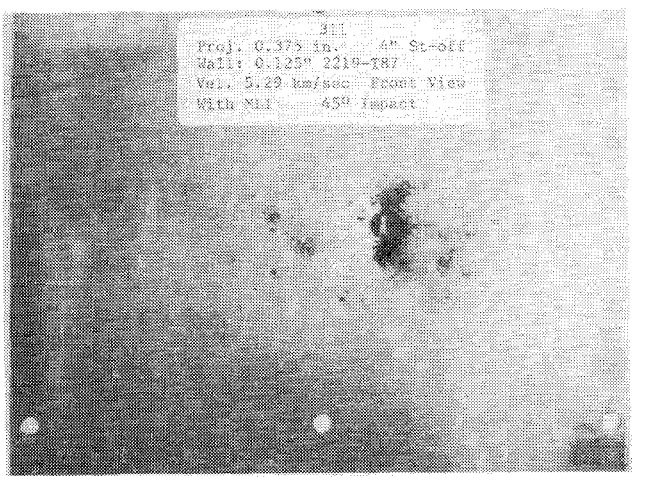

Fig. 8 Front view of a pressure wall plate of a corrugated bumper system under oblique impact.

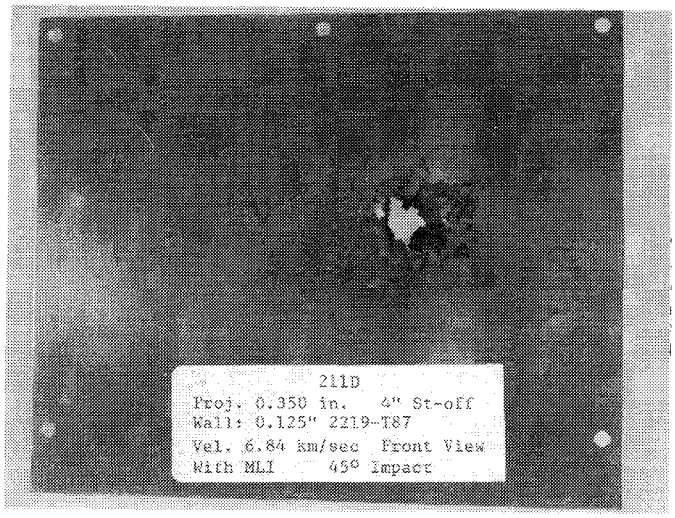

Fig. 9 Front view of a pressure wall plate of a monolithic bumper system under oblique impact.

perforation under oblique impact was possible in both system types, it occurred with a much lower frequency and was much less severe in corrugated bumper systems than in the monolithic bumper systems.

The increased protection against pressure wall plate perforation under oblique impact provided by the shallow corrugated bumpers as compared to the corresponding monolithic bumpers is also evident in Fig. 4. The area between the two penetration functions represents those 45 deg impacts that would perforate a pressure wall plate protected by a monolithic bumper but would not perforate a pressure wall plate protected by a shallow corrugated bumper similar in design to the ones used in this study.

In Table 4 it can also be seen that the total damage on the front surfaces of the pressure wall plates in the corrugated bumper systems under oblique impact were also generally smaller than those in the corresponding systems with monolithic bumpers. However, it is again noted that the smaller damage areas in the corrugated bumper systems were not due to a concentration of the debris clouds. Rather, the reduced damage areas were due to the decrease in the quantity of bumper and projectile debris fragments that constituted the debris cloud and eventually struck the pressure wall plate.

Finally, it is noted that in approximately half of the corrugated bumper systems under oblique impact, there was absolutely no damage to the pressure wall plate along the "normal" debris trajectory. This phenomenon occurred only once in the dual-wall systems with monolithic bumpers (Table 4). Since the MLI was present in both types of systems, it would appear that the corrugated bumpers absorbed a significant portion of normally directed energy. This feature would serve to further lessen the likelihood of pressure wall plate perforation and would also reduce the magnitude of front surface damage on the pressure wall plates.

Optimization of Corrugated Bumper Plate Design

Introductory Comments

In the previous section, the use of corrugated bumper plates in dual-wall systems was shown to increase the resistance of such systems against perforation by hypervelocity projectiles. However, use of the corrugated bumper plate in its present configuration can still lead to serious problems. Because of its flat front plate, if the corrugated bumper plate is impacted obliquely by a hypervelocity projectile, a significant amount of damaging ricochet debris will be created.[9] These high-speed ricochet debris particles can destroy external spacecraft subsystems, which may also result in catastrophic failure and loss of life. Uncontained ricochet debris particles also increase the contamination of the orbital environment and can pose a threat to future missions into that environment. Since the majority of on-orbit impacts are expected to occur at oblique angles, the creation of ricochet debris is an issue that must be addressed. In a previous paper,[20] the design of an external shield system that would contain the ricochet debris created in an oblique hypervelocity impact was presented. In this section, the design of the corrugated bumper plate is modified and optimized so that the potential for the creation of ricochet debris in the modified corrugated bumper configuration is significantly less that that of the original corrugated bumper configuration.

Minimization of Ricochet Debris Creation

The first step in the modification of the corrugated bumper plate design to reduce its potential for ricochet debris creation is to remove the front plate. However, in order not to diminish the protection afforded to the pressure wall, the front plate is not eliminated from the structural system, but merely moved to a new location between the modified corrugated bumper plate and the pressure wall plate. The exact placement of this plate within this space depends on the nature of the threat against which the pressure wall must be protected and is beyond the scope of this paper.

The next step is to optimize the rise angle α of the corrugations in the modified corrugated bumper plate. The objective of the optimization process is to find an angle α such that the amount of ricochet debris created by an oblique hypervelocity impact is minimized. A schematic of such an impact is shown in Fig. 10. From Fig. 10 it can be seen that ricochet debris can be created in two ways. First, by the primary impact of the original projectile on one of the faces of the modified corrugated bumper plate, and second, by the secondary impacts of ricochet debris particles on an adjacent corrugation face. Based on the fact that little or no ricochet debris is created when a projectile strikes a flat plate along normal or near-normal trajectories, in order to minimize the potential for ricochet debris creation, the normal components of the primary and secondary debris impacts must be maximized. This maximization is accomplished as follows.

Consider the primary impact of a projectile on a modified corrugated bumper plate and the secondary impact of a resulting ricochet debris particle at points X and Y, respectively, as shown in Fig. 10. In Fig. 10, γ is the angle between the spacecraft velocity vector and the projectile trajectory, θ is the angle between the outward pointing normal of the impacted corrugation face and the trajectory of the parent projectile, V_r is the velocity of the ricochet debris particle, and η is the angle characterizing the trajectory of the ricochet debris particle with respect to the corrugation face that sustained the primary impact. The impact velocity of the original projectile is given by

$$V = 2V_s \cos\gamma \tag{1}$$

where V_s is the spacecraft orbital velocity.[18] Using simple geometry, it can be shown that

$$\theta = \alpha - \gamma \quad \text{if } -\alpha < \gamma < \alpha \tag{2a}$$

$$\theta = \gamma - \alpha \quad \text{if } -\pi/2 < \gamma < -\alpha \text{ or if } \alpha < \gamma < \pi/2 \tag{2b}$$

For the purposes of this investigation, the impact velocities of the original projectile and the ricochet debris particles are assumed to adequately characterize the primary and secondary impacts on the appropriate faces of the modified corrugated bumper plate. Impact energy and momentum are not used because, unlike impact velocity, the mass distribution of the orbital debris environment cannot be easily characterized as a function of the angle γ. The normal velocity components of the primary and secondary impacts are considered one at a time in the following paragraphs and then summed together

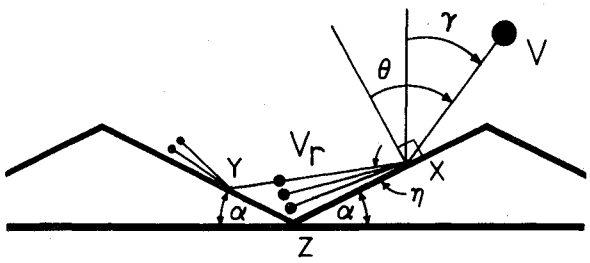

Fig. 10 Debris particle trajectories and parameters for corrugated bumper system optimization.

Table 5 Optimum corrugation rise angle (α) values for V_s = 8 km/s

	Ricochet particle trajectory η, deg		
V_r, km/s	20 deg	25 deg	30 deg
1	38.9	39.6	40.2
2	42.6	43.7	44.8
3	45.0	46.4	47.7

to yield the total normal velocity component that must be maximized.

First, the normal velocity component of the primary impact that is to be maximized is the sum of the normal velocity components from all possible impacts on a pair of adjacent corrugation faces and, as such, is given by

$$V_1 = \int_{-\pi/2}^{\pi/2} V_{np}\, d\gamma \tag{3}$$

where V_{np} is the normal component of the projectile impact velocity V and is given simply by

$$V_{np} = V \cos\theta \tag{4}$$

Substituting Eq. (1) into Eq. (4) and the result into Eq. (3) yields

$$V_1 = 2\int_0^{\pi/2} 2V_s \cos\gamma \cos\theta\, d\gamma \tag{5}$$

where the limits of integration have been changed and a factor of two has been added because of symmetry considerations.

Second, from triangle XYZ in Fig. 10, the normal component of the impact velocity V_r of a secondary impact that is associated with a primary impact that occurred at an angle γ can be shown to be given by

$$V_{ns} = V_r \sin(2\alpha - \eta) \tag{6}$$

where V_r and η are typically functions of the angle γ. Thus, the secondary normal velocity component to be maximized is the sum of all such V_{ns}:

$$V_2 = 2\int_0^{\pi/2} V_{ns}\, d\gamma \tag{7}$$

Substituting Eq. (6) into Eq. (7) yields

$$V_2 = 2\int_0^{\pi/2} V_r \sin(2\alpha - \eta)\, d\gamma \tag{8}$$

Although V_r and η are typically functions of γ, previous research into the damage potential of ricochet debris particles has shown that for hypervelocity impacts the speed of the most damaging ricochet debris particle and the trajectory of the farthest ricochet debris particle are relatively independent of the trajectory obliquity of the parent projectile.[20] Thus, if the secondary impact is assumed to be that of the ricochet debris particle whose trajectory is farthest from the initially impacted corrugation face, then the integrand in Eq. (8) is constant with respect to γ. This allows a simple evaluation of the integral itself, that is

$$V_2 = \pi V_r \sin(2\alpha - \eta) \tag{9}$$

Since each primary impact has a secondary impact associated with it, the total function to be maximized is given by the sum of V_1 and V_2. Thus, combining Eqs. (5) and (9) yields

$$V_n = 2\int_0^{\pi/2} 2V_s \cos\gamma \cos\theta\, d\gamma + \pi V_r \sin(2\alpha - \eta) \tag{10}$$

Making use of the relationship between θ and γ given in Eqs. (2a) and (2b) and the fact that for a given orbit the spacecraft velocity is constant, Eq. (10) can be rewritten as

$$V_n = 4V_s\int_0^{\alpha} \cos(\alpha - \gamma)\cos\theta\, d\gamma + 4V_s\int_{\alpha}^{\pi/2} \cos(\gamma - \alpha)\cos\theta\, d\gamma + \pi V_r \sin(2\alpha - \eta) \tag{11}$$

Using $\cos(\alpha - \gamma) = \cos(\gamma - \alpha)$, Eq. (11) can be simplified and readily evaluated to yield

$$V_n = V_s(2\sin\alpha + \pi\cos\alpha) + \pi V_r \sin(2\alpha - \eta) \tag{12}$$

This is the equation that must be maximized with respect to α in order that the modified corrugated bumper design be one in which the creation of ricochet debris particles is minimized. Following standard maximization techniques, we have

$$\frac{\partial V_n}{\partial \alpha} = V_s(2\cos\alpha - \pi\sin\alpha) + 2\pi V_r \cos(2\alpha - \eta) = 0 \tag{13}$$

In order to be able to solve this equation for α, the quantities V_r, V_s, and η must be known. Following the results obtained previously,[20] it is assumed for the purposes of this investigation that V_r = 2 km/s and that η = 30 deg. For a spacecraft velocity of 8 km/s, solving Eq. (13) for α yields α = 44.8 deg. This is the value of the modified corrugated bumper plate rise angle that will, for the assumed values of V_r, V_s, and η, minimize the potential for the creation of ricochet debris in the event of an oblique hypervelocity impact.

Since the value of α = 44.8 deg was based on a specific set of values for V_r, V_s, and η, it would be instructive to see how this optimum α value changes when other reasonable choices of V_r, V_s, and η are used. Table 5 shows the resulting values of α for V_r = 1, 2, 3 km/s, η = 20 deg, 25 deg, 30 deg, and for a constant spacecraft velocity of 8 km/s. As can be seen in this table, the optimum value of α is relatively independent of the assumed value of η and only has a slight dependence on the initial choice of V_r. Deviations from the α value calculated with V_r = 2 km/s and η = 30 deg are seen to be highest at large values of η and lowest at small values of η. However, since deviations on the order of $\pm 10\%$ are possible, additional research must be performed to characterize more accurately the dependence of V_r and η on the impact parameters of the parent projectile. This will result in a refined optimum value of the rise angle α for minimum ricochet debris generation.

Conclusions

An investigation of the hypervelocity impact response of dual-wall structures with corrugated and monolithic bumpers has revealed many interesting response characteristics. Based

on the observations made during the course of this study, it appears that a significant increase in protection against perforation by hypervelocity projectiles can be achieved if the traditional monolithic bumper in a dual-wall configuration is replaced with a corrugated bumper of equal or near-equal weight. In the specimens with corrugated bumpers, the frequency of pressure wall plate perforation was significantly lower than in corresponding specimens with monolithic bumper plates. Additionally, the damage area on the pressure wall plates was significantly decreased when a monolithic bumper plate was replaced with an equal-weight corrugated bumper plate. Use of corrugated bumper plates also decreased the possibility of pressure wall plate rear-side spall, especially under normal impact. A procedure was developed with which the configuration and the parameters of the corrugated bumper plate could be modified in order to reduce the potential for the creation of ricochet debris in the event of an on-orbit impact. The procedure is straightforward and can be used with a variety of threat environments to yield an optimum corrugation design.

Acknowledgments

The authors are grateful for support from the NASA Marshall Space Flight Center under Contract NAS8-36955/DO16 and would like to acknowledge the assistance of Alan Bean during the data acquisition phase of this investigation. The authors also wish to express their appreciation to Hubert Smith, Joe Lambert, and Roy Taylor of the Laboratory Support Branch of the NASA/MSFC Materials and Processes Laboratory, to Phillip Petty and Robert Stowell of the Martin Marietta Corporation, and to Ben Ramsey and Earl Shirley of the Boeing Corporation for conducting the impact testing that made the experimental portion of this report possible.

References

[1]Whipple, F. L., "Meteorites and Space Travel," *Astronomical Journal*, Vol. 52, 1947, p. 137.

[2]Wallace, R. R., Vinson, J. R., and Kornhauser, M., "Effects of Hypervelocity Particles on Shielded Structures," *ARS Journal*, 1962, pp. 1231–1237.

[3]Maiden, C. J., Gehring, J. W., and McMillan, A. R., "Investigation of Fundamental Mechanism of Damage to Thin Targets by Hypervelocity Projectiles," GM-DRL-TR-63-225, General Motors Defense Research Lab., Santa Barbara, CA, Sept. 1963.

[4]Maiden, C. J., and McMillan, A. R., "An Investigation of the Protection Afforded a Spacecraft by a Thin Shield," *AIAA Journal*, Vol. 2, 1964, pp. 1992–1998.

[5]D'Anna, P. J., "A Combined System Concept for Control of the Meteoroid Hazard to Space Vehicles," *Journal of Spacecraft*, Vol. 2, 1965, pp. 33–37.

[6]Nysmith, C. R., "An Experimental Impact Investigation of Aluminum Double-Sheet Structures," *Proceedings of the AIAA Hypervelocity Impact Conference*, AIAA Paper 69-375, 1969.

[7]Cour-Palais, B. G., "Hypervelocity Impact in Metals, Glass, and Composites," *International Journal of Impact Engineering*, Vol. 5, 1987, pp. 221–237.

[8]Coronado, A. R., Gibbins, M. N., Wright, M. A., and Stern, P. H., "Space Station Integrated Wall Design and Penetration Damage Control," D180-30550-1, Boeing Aerospace Co., Seattle, WA, July 1987.

[9]Schonberg, W. P., and Taylor, R. A., "Penetration and Ricochet Phenomena in Oblique Hypervelocity Impact," *AIAA Journal*, Vol. 27, 1989, pp. 639–646.

[10]Posever, F. C., Rish, F. L., and Scully, C. N., "Impact Effects on Meteoroid Shielding Configurations for Velocities up to 60,000 fps," *Journal of Spacecraft*, Vol. 2, 1968, pp. 738–741.

[11]Schonberg, W. P., "Hypervelocity Impact Penetration Phenomena in Aluminum Space Structures," *Journal of Aerospace Engineering*, Vol. 3, 1990, pp. 173–185.

[12]Richardson, A. J., and Sanders, J. P. "Development of Dual-Bumper Wall Construction for Advanced Spacecraft," *Journal of Spacecraft*, Vol. 9, 1972, pp. 448–451.

[13]Schonberg, W. P., "Hypervelocity Impact Response of Spaced Composite Material Structures," *International Journal of Impact Engineering*, Vol. 10, 1990, pp. 509–523.

[14]Riney, T. D., and Halda, E. J., "Effectiveness of Meteoroid Bumpers Consisting of Two Layers of Distinct Materials," *AIAA Journal*, Vol. 6, 1968, pp. 338–344.

[15]Hopkins, A. K., Lee, T. W., and Swift, H. F., "Material Phase Transformation Effects upon Performance of Spaced Bumper Systems," *Journal of Spacecraft*, Vol. 9, 1972, pp. 342–345.

[16]Swift, H. F., and Hopkins, A. K., "Effect of Bumper Material Properties on the Operation of Spaced Meteoroid Shields," *Journal of Spacecraft*, Vol. 7, 1970, pp. 73–77.

[17]Taylor, R. A., "A Space Debris Simulation Facility for Spacecraft Materials Evaluation," *SAMPE Quarterly*, Vol. 18, 1987, pp. 28–34.

[18]Kessler, D. J., Reynolds, R. C., and Anz-Meador, P. D., "Orbital Debris Environment for Spacecraft Designed to Operate in Low Earth Orbit," NASA TM 100471, Houston, TX, 1989.

[19]Morrison, R. H., "A Preliminary Investigation of Projectile Shape Effects in Hypervelocity Impact of a Double Sheet Structure," NASA TN D-6944, Washington, DC, 1972.

[20]Schonberg, W. P., and Taylor, R. A., "Exterior Spacecraft Subsystem Protective Shielding Analysis and Design," *Journal of Spacecraft and Rockets*, Vol. 27, 1990, pp. 267–274.